Nuclear Inst. and Methods in Physics Research, A 1048 (2023) 168007

Contents lists available at ScienceDirect

Nuclear Inst. and Methods in Physics Research, A

journal homepage: www.elsevier.com/locate/nima

Full Length Article

CARME — The CRYRING Array for Reaction MEasurements

A new approach to study nuclear reactions using storage rings

C.G. Bruno [a,*], J.J. Marsh [a], T. Davinson [a], P.J. Woods [a], P. Black [a], A. Bräuning-Demian [b], J. Glorius [b], A. Grant [c], O. Hall [a], A. Headspith [c], P. Hindley [c], I. Lazarus [c], K. Middleman [c], N. Petridis [b], M. Lestinsky [b], Yu.A. Litvinov [b], R.S. Sidhu [a], T. Stöhlker [b,d]

[a] School of Physics and Astronomy, The University of Edinburgh, Peter Gurthrie Tait Road, EH9 3FD, Edinburgh, UK
[b] GSI Helmholtzzentrum für Schwerionenforschung GmbH, Planckstr. 1, 64291, Darmstadt, Germany
[c] UKRI STFC Daresbury Laboratory, Keckwick Lane, WA4 4AD, Daresbury, Warrington, UK
[d] Helmholtz-Insitut Jena, Fröbelstieg 3, 07743, Jena, Germany

ARTICLE INFO

Keywords:
Storage rings
Nuclear astrophysics
XHV
Silicon detectors

ABSTRACT

The low-energy CRYRING@ESR storage ring, recently commissioned at GSI@FAIR (Germany), is a world-unique facility able to decelerate and store beams produced in-flight to energies $E \leq 10$ MeV/u. CRYRING@ESR offers the unique opportunity to exploit high quality, pure, radioactive beams of species difficult to produce via the ISOL method for reaction studies directly at energies of astrophysical interest. The use of thin, pure, windowless in-ring targets combined with the re-circulating beam also presents significant advantages in terms of background and luminosity. This paper describes a new modular nuclear and atomic physics detection array, CARME (CRYRING Array for Reaction MEasurements), specifically designed to allow these investigations to be carried out for the first time in the Extreme High Vacuum (XHV) environment of the CRYRING@ESR. CARME mounts a high granularity silicon strip detector system adapted for XHV conditions, and will be used for high resolution direct and indirect charged particle reaction studies.

1. Introduction

Nuclear reaction measurements near and below the Coulomb barrier (E∼ MeV) using radioactive isotope beams are a powerful tool to investigate key nuclear properties and cross-sections, to improve our fundamental understanding of the atomic nucleus, and our knowledge of nuclear properties of interest in *e.g.* astrophysical scenarios, medical physics, and the nuclear fuel cycle. However, some key investigations involving radioisotopes remain impossible due to the difficulty of producing some radioactive beams with sufficient intensity and purity using extant methods. For example, the traditional ISOL (Isotope Separation On-Line) approach can provide very good intensity, isotopic purity, and emittance but available beams are limited to those radioactive elements which can diffuse out of a production target before decaying. On the other hand, the competing in-flight technique can produce in principle any isotope of interest, but limited intensity, purity and emittance hamper scientific exploitation at Coulomb barrier energies. Improving beam quality and intensity is key to unlock solutions to long-standing scientific puzzles. In response to this need, new facilities and radioactive beam techniques are being developed around the world. A new, extremely promising approach consists in storing radioactive heavy ions inside a ring, where they impinge on a pure in-ring target. Un-reacted ions are recirculated again and again, interacting with the target every cycle. This results in orders-of-magnitude increase in effective beam intensity, a game-changer for radioactive beam investigations. Re-circulation also enhances the isotopic purity of the stored beam, as only ion species with the correct charge to mass ratio survive in the beam orbit. Furthermore, each cycle, small energy losses suffered by the circulating beam are compensated by an *electron cooler*, a device which is capable to compensate for the energy losses due to beam collision with rest gas and target, and reduces emittance. Storage rings ideally compensate for the main weaknesses of radioactive beams produced in-flight, and allow the use of uniquely pure, intense beams of previously unavailable ion species, as well as versatile beam handling and manipulation [1].

The main challenge in carrying out nuclear physics measurements at heavy ion storage rings is to use as much of the injected beam as possible, which requires to keep the ions circulating with little to no losses. To achieve this aim requires extremely good levels of vacuum inside the ring, typically better than 10^{-10} mbar, a very significant technological challenge for experiments. The internal target itself is

* Corresponding author.
E-mail address: carlo.bruno@ed.ac.uk (C.G. Bruno).

https://doi.org/10.1016/j.nima.2022.168007
Received 19 November 2022; Received in revised form 23 December 2022; Accepted 28 December 2022
Available online 9 January 2023

an unavoidable obstacle to the ion path, which limits the maximum target thickness that can be usefully employed. Experiments must strike a balance between target thickness and ion loss per revolution. More details are given in the next section.

Using rings for nuclear reaction measurements was pioneered at the Experimental Storage Ring (ESR) at GSI Laboratory (Germany) using radioactive ions produced via in-flight fragmentation and separated in the FRagment Separator (FRS). First measurements were carried out by the EXL collaboration (EXotic nuclei studied in Light-ion induced reactions), using a complex array of detectors outside of the ring ultra-high vacuum (UHV), except for one (later two) small position-sensitive Si(Li) detectors acting as vacuum pocket windows [2,3]. The setup was commissioned using 350 MeV/u ^{135}Xe and ^{135}I beams. It was later used for a ^{58}Ni(α, α)^{58}Ni investigation at E≥100 MeV/u aimed at studying the nuclear structure of ^{58}Ni [4,5], and of the doubly-magic radioactive ^{56}Ni via ^{56}Ni(p, p)^{56}Ni [6]. A similar technique was used at the CSR (Cooler Storage Ring) at HIRFL (Heavy Ion Research Facility Lanzhou, China) to study the ^{58}Ni(p, p)^{58}Ni [7]. More recently, an investigation of the astrophysically relevant ^{15}O(α, γ)^{19}Ne reaction was attempted via the ^{20}Ne(p, d)^{19}Ne transfer reaction in a proof of principle experiment at the ESR using two Double-sided Silicon Strip Detectors (DSSD) as ΔE-E telescope [8]. Proton capture reactions are routinely studied at the ESR employing a position-sensitive Double-sided Silicon Strip Detector (DSSD) placed after one of the ESR magnetic dipoles. Nuclear reaction products were separated from un-reacted beam ions based on their charge-to-mass ratio inside the dipole. This technique was first tested with a stable ^{96}Ru beam at 9–11 MeV/u [9], and later with a long-lived ($t_{1/2}$ = 1.8 × 10^{22} years) radioactive ^{124}Xe beam down to 5.5 MeV/u [10]. The ^{124}Xe(p, γ)^{125}Cs reaction is key in the astrophysical γ-process occurring in supernova explosions, and the stored ion energies at the ESR corresponded to the high tail of the astrophysically relevant Gamow window for the ensuing supernova explosion. More investigations using this latter technique are planned in the near future.

Studying nuclear reactions at heavy ion storage rings offers a wealth of new possibilities. To exploit these opportunities, new rings are being considered for construction around the world, *e.g.* in TRIUMF (Canada) [11] and CERN [12]. This work will describe specifically the commissioning of the CRYRING Array for Reaction MEasurement (CARME), at the low-energy CRYRING storage ring [13–16], part of FAIR [17,18] at GSI. CARME is a purpose-built detection array funded by the UK Science and Technology Facilities Council [19] to carry out high-resolution measurements of nuclear reactions using radioactive ions stored at CRYRING. This is at present the only ring in the entire world where radioactive beams produced in-flight can be stored and decelerated at energies $E \ll 10$ MeV/u, allowing measurement of nuclear reactions at or below Coulomb barrier energies, using pure radioactive beams of species unavailable elsewhere. CARME was designed for high-energy and angular resolution studies of nuclear reactions either upstream, or downstream, or both of an in-ring cryogenic jet target mounted at CRYRING.

This work will introduce the unique conditions at which nuclear reactions must be carried out at CRYRING, describe the aims behind the novel design of the CARME detection array, and detail its commissioning.

2. Nuclear reactions at CRYRING

The energy range ions can be stored in a ring is mostly determined by the maximum beam rigidity and stability of the power supplies. In particular, CRYRING can accept beam at energies approximately $0.01 \leq E \leq 10$ MeV/u depending on the ion species. Ions can be injected in one of two ways. First, the ring can be filled using a low-energy ($E \simeq 30 - 300$ keV) off-line, dedicated local ion source which can provide most stable isotopes. In addition to being extremely valuable for commissioning purposes, CRYRING is such a unique facility world-wide that ground-breaking experiments can be carried out even with stable beams. A local ion source unlocks the possibility to carry out a cutting-edge science programme at CRYRING in parallel and independently of the rest of the GSI/FAIR facility. While at present only stable isotopes can be injected into CRYRING from this local source, there are plans to replace it with a source capable of accelerating long-lived isotopes such as *e.g.* ^{44}Ti ($t_{1/2}$ = 60 y) [20] further expanding the scientific capabilities of CRYRING in stand-alone mode.

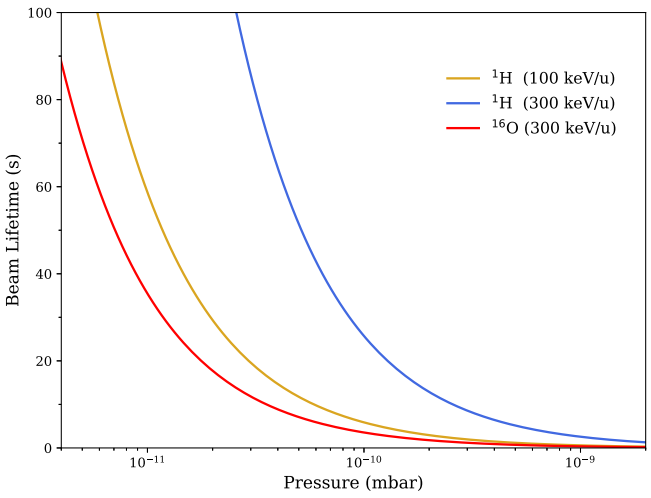

Fig. 1. Expected beam lifetime in seconds against the residual gas pressure for a typical residual gas pressure composition. A ^{16}O beam of 300 keV/u (red) and ^{1}H beams of 100 (gold) and 300 keV/u (blue) are shown. Typical pressures on the CRYRING are $< 5 \times 10^{-11}$ mbar to maximise the beam lifetime. Note the target is assumed to be off.

Radioactive beams produced in-flight can also be injected into CRYRING, however this production technique results in very high ion energies (E ≥ 100 MeV/u), which cannot be directly accepted and stored. Instead, in-flight beam must be first decelerated in the ESR (∼30 s) and pre-cooled and subsequently transferred to CRYRING for further deceleration to energies of interest, and further cooling (if required). This approach requires the combination of an in-flight facility linked to *two* storage rings with overlapping energy ranges, which is world-unique to GSI/FAIR. Although technically feasible, at the time of writing this has been tested in practice with a stable beam, but never with radioactive ions.

At typical storage energies of E ∼ MeV/u, ions will revolve with frequencies of the order of hundreds of kHz in CRYRING. This recirculation produces a boost in the effective beam intensity of the order ∼10^5, which is one of the key advantages in using storage rings. However, rings are a rather unique environment to carry out nuclear reaction measurements, and come with a set of technically challenging requirements for a detection array. In particular, at CRYRING, a key requirement is compatibility with the extreme high vacuum (XHV ∼10^{-12} mbar) environment necessary to keep heavy ions circulating at low energies as shown in Fig. 1. Note that while reaching UHV (10^{-10} mbar) is a challenge, it is considerably easier than achieving XHV which requires a much more stringent and limited selection of materials that can be placed under vacuum. CARME is the first nuclear physics detection array designed to fulfil XHV requirements, and develop technical solutions to satisfy these challenges.

2.1. Beam storage lifetime

Good vacuum is key for successful ring experiments. Any interaction between stored ions and the residual gas left after making a vacuum or any internal target, carries the probability of either scattering stored ions at very high angles, or causing a change in their charge state

(electron stripping or pick-up). In either case, the heavy ions are lost. A full description of the complex physics behind beam loss is beyond the scope of this work, see instead [12] and references within. Since this is a combination of stochastic processes, it is modelled via an effective lifetime which typically ranges from fractions of a second to a few minutes. In *typical* running conditions for nuclear physics reactions at CRYRING, the two dominant processes responsible for beam loss are elastic Rutherford scattering at angles outside of the ring acceptance, and capture of an electron by the stored ion (Electron Capture). The cross-section σ_{EC} associated to this second process can be modelled via the following semi-empirical equation [12,21]

$$\sigma_{EC} = 1.1 \times 10^{8} \frac{q^{3.9} Z_{gas}^{4.9}}{E^{4.8}} [\mathrm{cm}^2] \quad (1)$$

where q is the charge state of the stored ion, Z_{gas} is the atomic number of the atoms with which the ion interacts (*e.g.* the residual gas) and E is the energy of the stored ions expressed in keV/A. It is straightforward to see that beam energy plays a major role in the lifetime of the beam. Higher beam energy results in lower beam losses due to unwanted beam interactions, and ultimately higher integrated luminosity. Heavy ions in the residual gas, or the internal target, will result in higher beam loss. In order to compensate for the low energy at which ions are stored in CRYRING and keep the beam circulating it is especially crucial to minimise the amount of residual gas, and in particular any heavy components which are naturally present in air such as Argon. For this reason CRYRING is kept in XHV, and instrumentation placed inside the ring must avoid using materials that may release gases under vacuum, especially if this out-gassing would contain heavy atoms.

2.2. The internal target

The in-ring cryogenic micro-droplet target is a necessary obstacle to the beam path in nuclear reaction experiments. Technical details of this target are given in [22]. The micro-droplets are produced by super-cooling ultra-pure gas stored in bottles. Fresh gas is constantly injected and pumped out of the ring (at present without recirculation) and thus target composition and stoichiometry do not change over time. This is a major advantage over typical solid targets which require other chemical elements or a backing, and which degrade over time. However, the target can only be made out of elements that exist as gases. In order to keep Z_{gas} low to avoid losing beam ions (Eq. (1)), hydrogen (or deuterium) and helium are typically chosen. Although this may appear a serious limitation, nearly all nuclear astrophysics reactions involve at least one isotope of hydrogen or helium since these two elements make up the bulk of a star.

Typical densities which can be achieved with this type of target are of the order of $10^{11\sim14}$ atoms/cm^2 depending on the gas species, gas flow and target temperature. Higher densities would not necessarily improve the luminosity of a reaction measurement as they would cause the beam to be lost faster (*e.g.* lifetime $\ll 1$ second), potentially reducing the duty cycle of the measurement significantly (see later). However the uniquely low target density is compensated by beam recirculation, and has its own advantages. In particular, charged particles produced by nuclear reactions due to beam impinging on the target suffer from negligible energy loss or straggling when emerging from the target at any angle, and can be detected with extremely high energy and angular resolution. This is a key and unique advantage of charged particle spectroscopy at rings against traditional techniques.

2.3. Cooling the beam

When beam is first injected in a storage ring, it *typically* has a rather high emittance. This is especially true for in-flight beam due to the way it is produced. One can make use of an electron cooler to reduce beam emittance ("cooling the beam") and improve its quality. The CRYRING has an ultra-cold electron cooler [13,23] which is especially suited for low-energy beams typically allowing to achieve beam width of the order of $\sim$ 1 mm, and energy spread $\frac{\Delta E}{E} \sim 10^{-4}$ or better, after approximately 1 s of beam recirculation. The possibility to use in-flight radioactive beams of such high quality is completely unique to rings. It is important to note that as a result of the change of beam emittance at injection and after recirculation, there are effectively two experimental conditions that a charged-particle detection array located inside a storage ring, like CARME, must work in. When un-cooled beam is first injected it is wide, and detectors must be out of the rather large beam path. After it is cooled, the beam becomes narrow and detectors must *move* closer to the beam axis to detect charged particles emitted at forward or backwards angles. This motion must occur under XHV conditions, synchronous with each injection cycle (few seconds typically), and is a non-trivial technical challenge.

2.4. Experiment design considerations

In summary, beam can be injected in CRYRING from either a local ion source, or in-flight beam can be transferred from the ESR. Beam preparation plus cooling typically takes 1–2 s. The internal target is kept off to avoid worsening the vacuum and the storage lifetime until beam is ready and cooled (if cooling is required). Then beam impinges on the target, decreasing the storage lifetime, and when too many ions have been lost the beam is dumped, the target is switched off, and the ring must be refilled. Deciding when to dump the beam depends on achieving optimal duty cycle (measurement time over beam preparation time), and is generally done on-line observing the beam storage lifetime. Typically, the beam is dumped after around one or two lifetimes. Given beam preparation times are of the order of a few seconds, lifetimes $\ll 1$ s will result in very low duty cycles (few percent, or less) and are not suitable for storage rings. This applies both for storage and for radioactive lifetimes.

In order to maximise the luminosity of a nuclear reaction measurement at a low-energy heavy ion storage ring like CRYRING, one typically wants to maximise the stored beam energy and avoid heavy ion species as target or stored ions. Heavy projectile on light target (*i.e.* inverse kinematics) almost always result in better lifetimes than the opposite because of the higher beam energies, and the fact that the lifetime dependency on the atomic number of the target is usually steeper than that on the charge state of the ion (*e.g.* Eq. (1)). Furthermore one should ensure optimal vacuum conditions with careful choice of materials and pumping systems and select radioisotopes with lifetimes ≥ 1 s. Of course, depending on the experiment, some of the criteria may need to be relaxed.

The main advantage of nuclear reaction measurements at rings are the high intensity, high purity, low emittance radioactive beams produced in-flight, impinging on an ultra-pure, ultra-thin, windowless target from which charged particle may be extracted with negligible energy degradation. CARME's design was optimised to exploit these advantages and carry out ultra-high resolution studies of nuclear reactions, at very small forward or backward angles close to the beam axis. High-resolution is mandatory to extract nuclear spectroscopic properties, but also to minimise background and to ensure the correct identification of signal peaks. Due to the need to operate in XHV, which takes weeks to months to achieve (see later), CARME was designed as a modular, flexible system which can accommodate a large range of potential measurements both for nuclear and for atomic physics. At present, the bulk of CARME's science programme consists in measurement for nuclear astrophysics, since the energy range at CRYRING is ideal to probe nuclear reactions directly inside the Gamow window.

3. CARME@CRYRING

A cut-away render and a photo of CARME mounted on the CRYRING are shown in Fig. 2. CARME is comprised of an interaction chamber which lies between the two parts (inlet and dump) of the internal target

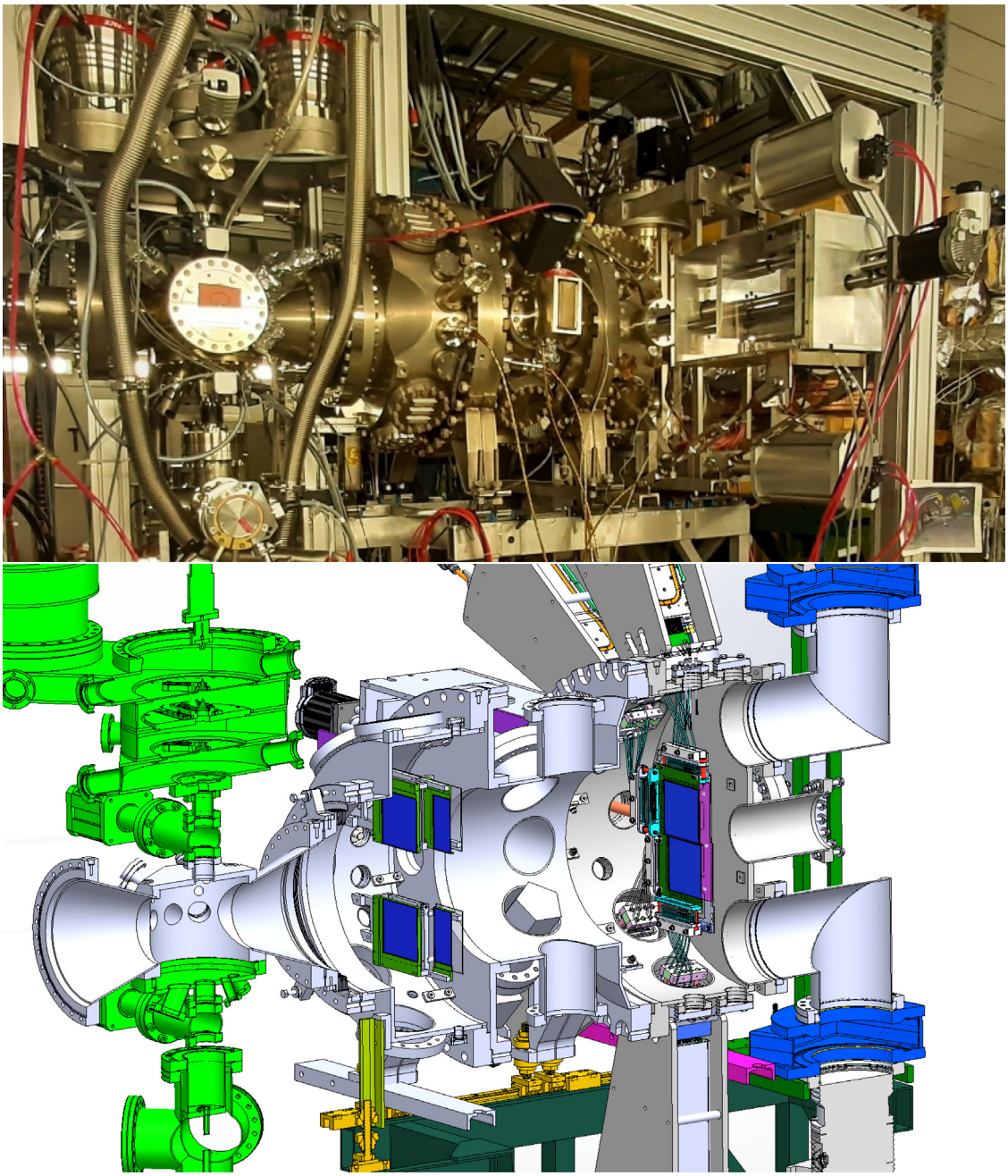

Fig. 2. (Top) photo and (bottom) render of CARME mounted on the CRYRING from approximately the same angle. Beam goes from the left to the right, and interacts with the internal target that is shown in green, mounted on the CARME interaction chamber (not green). Four of the six DSSD in the wall section, downstream from the interaction chamber, and two of the moving DSSD further downstream are shown. Also see Fig. 3.

(Fig. 2 green), and a main section to detect reaction products that can be mounted up- or down-stream of the interaction chamber. The vacuum vessels were manufactured by ITL Vacuum Components [24]. In Fig. 2 CARME is mounted downstream. The interaction chamber provides ±20 degrees line of sight upstream and downstream from the DSSDs to the gas jet target and has multiple ports on which beryllium windows, or optical windows can be mounted. This main section is further divided in three sub-sections. The closest to the target houses up to 6 static DSSDs covering the laboratory angular range ∼5–17 degrees. The following intermediate section houses no detectors and only provides additional space for pumps to be installed. Finally, the last section houses up to 4 moving DSSDs (Fig. 3) mounted on actuator arms. The angular coverage of the moving DSSDs is dependent on their position with respect to the beam axis, when positioned closest to the beam axis the laboratory angular range is from ∼0.5–7.5 degrees. Moving DSSDs are a necessity to cover angular ranges close to the beam axis when dealing with the cooled/uncooled beam. All materials and instrumentation were carefully selected and processed (see later). Achieving XHV is a rather complex procedure involving conventional pumps (*i.e.* oil-free scroll and turbo-molecular pumps) down to $\sim 10^{-9}$ mbar, followed by baking and passive NEG (Non-Evaporable Getter) and ion pumps. Normally one has to minimise the vacuum load as much as possible to stand a chance of achieving such high levels of vacuum. However, this was not an option for CARME due to the necessity of having DSSDs and electronic wires directly in XHV. To our knowledge, this is the first time moving DSSDs and such a high vacuum load have been used in XHV conditions. The next sections describe the components and processes adopted to achieve XHV.

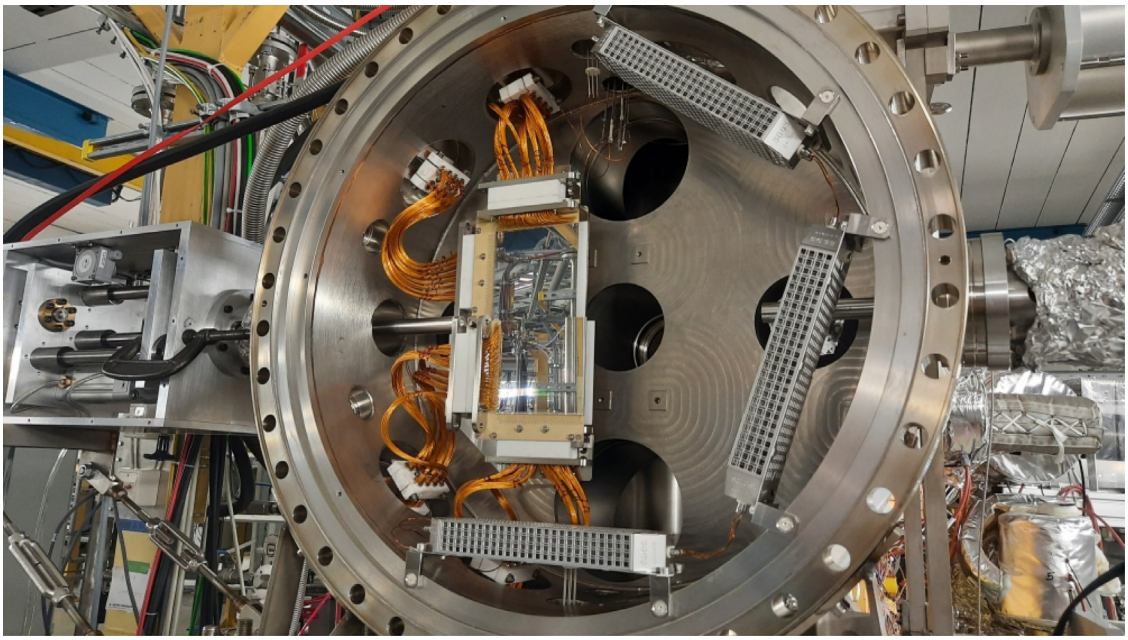

Fig. 3. A photo of the moving DSSD section of CARME, showing two DSSDs mounted on an XHV actuator arm, Kapton wires going to XHV feedthroughs, and three NEG strips mounted on the rim of the chamber. Two more getters that sit on the left hand side were temporarily removed for ease of installation. The photo is taken from the position of the target. The beam goes through the hole in the middle of the chamber.

3.1. Detectors

The detectors installed in CARME are 10 × 10 cm, 128 × 128 strip XHV-compatible DSSDs with wafer thicknesses of 1 mm, produced especially for this application by Micron Semiconductor Ltd [25]. Detectors have a strip pitch of 738 μm providing excellent angular resolution. The four moving DSSDs are placed 1057 mm from the gas jet target along the beam axis, while the front of DSSD wall is placed 483 mm away. We expect a nominal ∼ 25 keV FWHM energy resolution for ^{241}Am alpha particles. The silicon wafers are mounted in ceramic transmission carriers (1.6 mm Rogers 4003 material [26]) using UHV-rated silver loaded epoxy glue (Fig. 4). The contact pads of the silicon wafer are ultrasonically bonded to carrier contact pads. Traces run from the carrier contact pads to carrier vias into which Kapton wires are glued. Each side of the DSSD, corresponding to 130 Kapton coated wires, ends in a 137-way MACOR connector, followed by a MACOR strain relief (Fig. 5). The 130 wires are split in two 65 wires bundles, each of which ends in a 78-way MACOR connector that is plugged into two 78-way or three 78-way DN-100 vacuum feed-through flanges manufactured by Allectra.

3.2. XHV actuator arms

Each set of two moving detectors is mounted on an actuator arm (Fig. 6) which has a relative accuracy of 0.1 mm for the positioning of detectors. The two arms use a combination of a pneumatic cylinder (Festo Pneumatic Cylinder 50 mm Bore, 50 mm Stroke [27]), and a servo motor (Teknic CPM-SCSK-3432P-ELSA [28]) to actuate the motion attached to a leadscrew with 250 mm travel. In order to limit mechanical shock to the DSSDs during the actuator motion, the pneumatic cylinder is fitted with buffers to limit acceleration at the ends of the stroke. Furthermore, the pneumatic hoses contain check-needle valves to limit the rate of air admittance into the cylinder and thus the maximum velocity. The pneumatic motor is mounted on a moving plate that can be displaced by the servo motor. In turn, the pneumatic motor can push a second moving plate connected to a 316L stainless steel shaft which reaches the vacuum through a set of custom XHV bellows (96.5 mm stroke, 1 million cycles lifetime). DSSDs are mounted on a 316L stainless steel support, secured to the shaft. Two detectors are mounted on each support, for a total of four. A MACOR plate (≈ 1 mm thick) in the shape of two detectors combined was placed behind the detectors (partly visible in Fig. 3) to shield them from the heat generated by the NEG elements during activation. The displacement of the detectors is measured by a string potentiometer

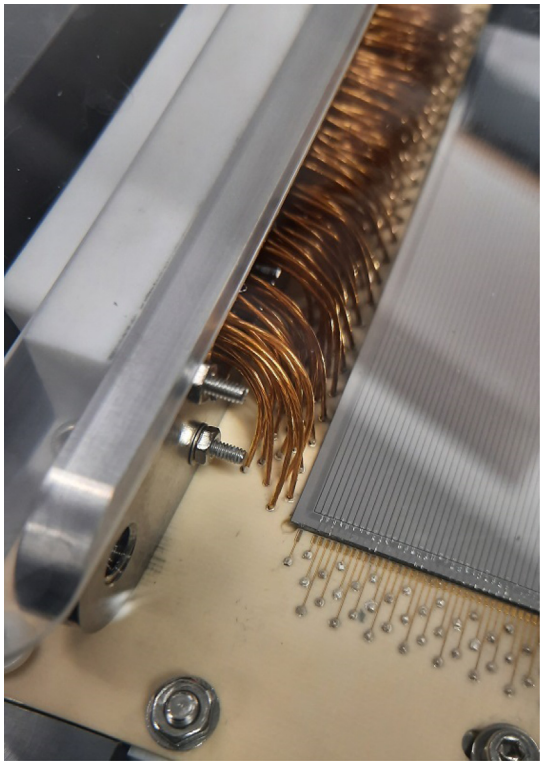

Fig. 4. Close-up photo of the bond wires and of the silicon strips of an XHV-compatible DSSD. Wires are 0.75 mm OD, Kapton insulated, silver plated copper wires (301-KAPM-060, Allectra).

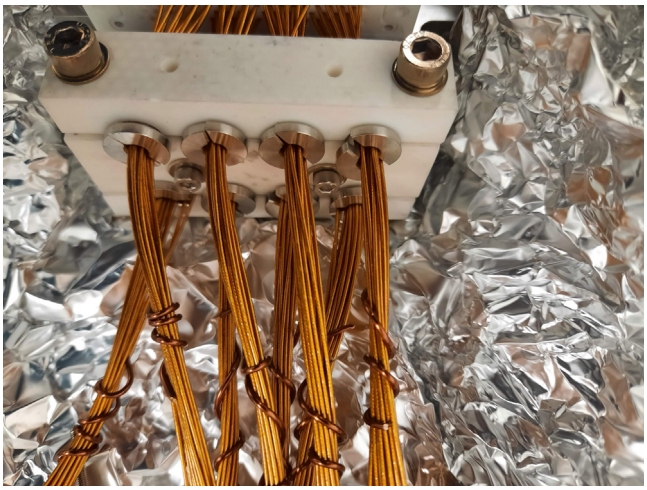

Fig. 5. Close up view of the MACOR strain reliefs mounted to the cable harnesses. Kapton cables are separated into bundles of 8–10 wires to be fed through strain relief. Additional stainless steel funnels were placed within strain reliefs to reduce wire stress.

(TE Connectivity SP1-4) with a precision of 0.1 μm. The motors system is controlled via a custom-written code, and can react automatically to ring events such as injection/dumping of the beam.

3.3. Data acquisition system

CARME uses the AIDA data acquisition electronics developed for high rates (~ 10 kHz per channel) in beta decay applications. A detailed description of electronics is given in Ref. [29]. Signal processing and data acquisition electronics are contained within Front End Electronics (FEE) modules mounted to the outside of the CARME chamber. Processing of signals is handled by four 16-channel Application Specific Integrated Circuits (ASICs). The ASICs contain two pre-amplifiers (for high and low/medium energy events), a shaping amplifier and discriminators. Selectable gain on the low/medium energy pre-amplifier allows for a Full Scale Range (FSR) of 20 MeV for the low energy channel or 1 GeV for the medium energy channel. The high energy channel has a 20 GeV FSR. The high energy channel is disconnected from the circuit until the low/medium energy channels are saturated. CARME will primarily utilise the low energy channel which has a nominal gain of ~ 0.7 keV per channel. ADC data is readout and stored in the Total Data Readout (TDR) GREAT data format [30]. The ADC data value, range indicator, channel number, FEE number and a partial timestamp are recorded in each data item. The full timestamp is reconstructed during merging of data from separate FEE modules by insertion of SYNC information data items, containing the time from an external white rabbit clock, into the data stream. Information data items are also used to store signals with the status of the moving detectors. Live monitoring of histograms and waveforms is available via the MIDAS Graphical User Interface [30].

3.4. Vacuum systems

The CARME detection chambers and the interaction chamber must achieve and maintain XHV conditions to operate on the CRYRING. In order to do so, the pumping speed installed in the vacuum chambers must be sufficient to remove molecules which out-gas from both the vacuum vessel and in-vacuum instrumentation. The largest source of out-gassing are the 261 m of 0.75 mm outer diameter, Kapton insulated, silver plated copper wires (301-KAPM-060, Allectra [31]) which connect the DSSDs to the signal feed-through flanges. Once baked, the out-gassing rate of the Kapton insulation is expected to be $\leq 1 \times 10^{-10}$ mbar(l/s)cm^{-2} [32,33]. CARME can mount up two 300 litres per second (l/s) turbo-molecular pumps (Leybold MAG W 300i [34]), with rotors suspended by magnetic bearings (instead of traditional ball bearings), to remove the possibility of the vacuum vessel being contaminated by oil or material produced by the mechanical wear of bearings. All-metal (VAT [35]) gate valves are installed between the turbo-molecular pumps and the vacuum chamber, with an oil-free scroll pump (Edwards nXDS 15i [36]) and a residual gas analyser (RGA) connected to the backing line of the turbo. This combination of pumps can bring the CARME chambers from atmospheric pressure down to around 10^{-8} mbar in typically 2–3 days, at which point baking the vacuum vessel becomes necessary to further reduce the pressure (Section 4.3). During and after baking, thirteen Non Evaporable Getter (NEG) wafer modules (UHV1400, SAES Getters) and four NEG/Ion combination pumps (NEXTorr D2000, SAES Getters [37]) are used to achieve XHV. These pumps can achieve a total pumping speed of 26,200 l/s (H_2), 1400 l/s is provided by each UHV1400 NEG module and 2000 l/s for each D2000 NEG-ion pump. NEG elements work by passively capturing residual gas molecules by adsorption on the surface of the getter itself. Residual gas molecules chemically bind to the surface and dissociate producing an ion layer which diffuse into the bulk of the getter over time, preventing escape. Non-reactive gas species, such as noble gases, are unable to be removed by NEG pumps. The surface of NEG elements becomes saturated at non-UHV pressures and requires activation under UHV vacuum conditions at 550 °C to renew the surface and allow capture of gas species [38]. Ion Pumps

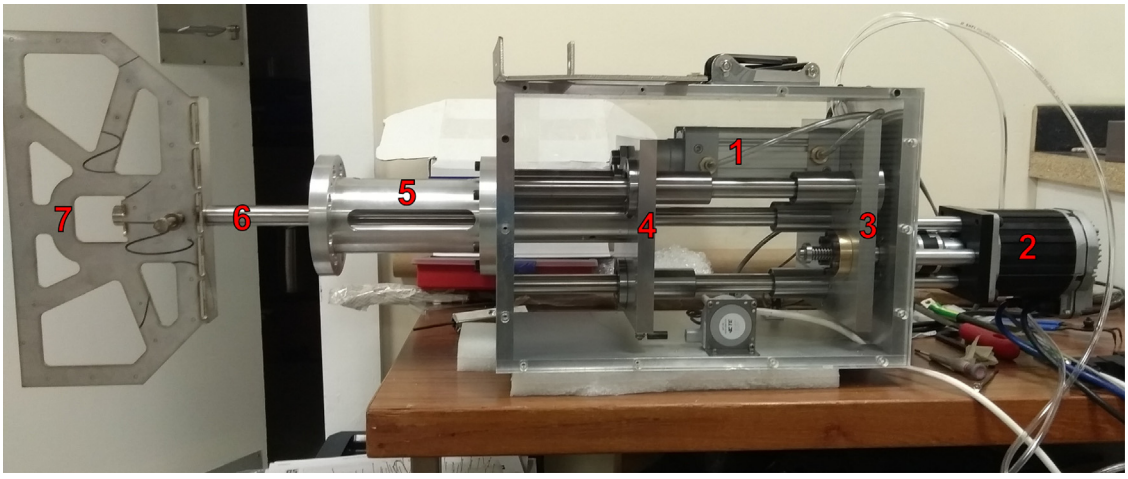

Fig. 6. Photo of the actuator arms with internal components labelled. Festo Pneumatic cylinder (1), Teknic CPM-SCSK-3432P-ELSA servo (2), first moving plate (3), second moving plate (4), metal shaft (5), space for XHV bellows (not mounted - 6), mounting plate for silicon detectors (temporary stand-in plate shown - 7). See text for details.

capture gas molecules by ion implantation. Gas is ionised within the ion pump cell and is then accelerated towards the cathode. The ions will either be buried below the cathode surface or sputter the reactive cathode material (usually titanium) onto surrounding surfaces which then acts as a getter to remove reactive residual gases [38]. A Hot Cathode gauge (Leybold Ionivac IE514) is installed on the chamber and is capable of measuring pressures down to 2×10^{-12} mbar.

4. Vacuum commissioning

Initial vacuum commissioning of the CARME vacuum chambers was carried out in the Accelerator Science and Technology Centre (ASTeC) at STFC Daresbury Laboratory (UK). Initial vacuum commissioning was conducted with no additional out-gassing load inside the chambers. Further commissioning with additional out-gassing load, first with Kapton cabling installed but no detectors and then with full instrumentation, were carried out directly on the CRYRING at FAIR.

4.1. Pre-processing of components

The CARME detection chamber, interaction chamber and all vacuum flanges were cleaned, placed in a large vacuum oven and heated to a maximum temperature of 1000 °C under vacuum for 2–4 h. This procedure, known as vacuum firing, permanently removes molecules, primarily hydrogen, trapped within the bulk of material, which would out-gas under XHV conditions, see Fig. 7. Signal feed-through flanges and other small components that could not be vacuum fired due to maximum temperature limitations were instead cleaned before installation in the chamber. The cleaning procedure consists of immersion in an ultrasonically agitated bath of Hydrofluoroether (HFE) 72DE followed by a vapour wash in HFE 72DE, each for 15 min. Components are then rinsed with a high pressure demineralised water jet at 80 °C before immersion in a ultra-sonically agitated bath of 60 °C alkaline de-greaser (P3 Almeco P36 or T5161) for 5 min. The components are finally rinsed with the water jet again and then dried with a clean air line. This cleaning procedure is outlined in the ASTeC cleaning procedures [39]. All components were wrapped in clean aluminium foils and stored in sealed plastic containers until installation. Smaller components were sealed under dry nitrogen within a polyethylene bag. All components were handled using polyethylene gloves. Prior to installation components were inspected for damage with particular attention paid to knife edges and sealing faces. All Kapton wires and MACOR ceramics used for detector cabling were cleaned and vacuum baked to a temperature of 200 °C for 48 h.

4.2. The bake-out tent

The ultimate pressure that can be achieved below UHV vacuum levels is limited by the out-gassing of gas molecules (primarily water molecules) which are weakly bound to internal chamber surfaces. The out-gassing rate of bound molecules is high enough to be detrimental to the level of vacuum but low enough that the vacuum level does not significantly improve over time. The out-gassing rate of surface adsorbed molecules has an exponential dependence on the temperature [40]. Baking the vacuum chamber at high temperature increases the out-gassing rate such that the majority of surface adsorbed molecules are removed from the chamber, reducing the vacuum level once the temperature has been reduced back to normal levels. Typically bake-out temperatures are in the range of 200–250 °C. The temperature of the bake-out for CARME is limited to 150 °C by micro-alloying of the DSSDs aluminium metalisation. During initial vacuum commissioning, a temperature of ∼ 150 °C was found to be sufficient to reduce out-gassing to achieve XHV conditions. In order to accommodate the complex shape of the CARME detection chamber, a custom aluminium frame and insulating jacket were constructed around CARME for the bake-out. The insulating jacket is composed of Polyurethane coated

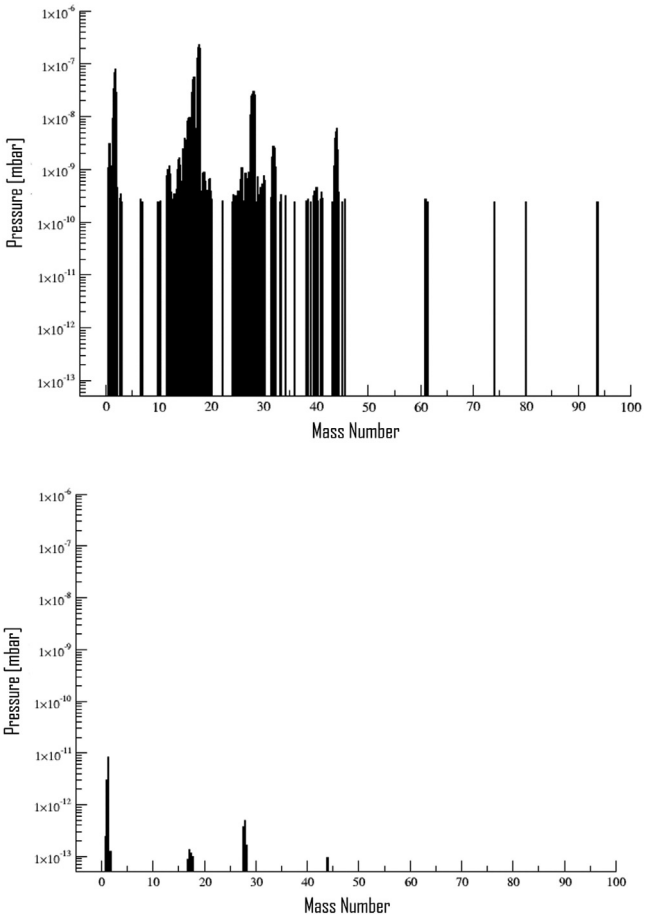

Fig. 7. RGA scans of the interaction chamber pre-vacuum-firing (top) and post-firing (bottom). Contributions from all masses are significantly reduced with most now below the sensitivity of the RGA probe. Minor residual species for H_2, N_2 and H_2O are present post-bake.

fibreglass cloth filled with 10 mm thick fibreglass needle mat felt insulation. This jacket is further insulated with an external layer of 0.45 mm aluminium coated fibreglass cloth, and an aluminium shell to secure the jacket in place. See Fig. 8. Eleven 250–500 W ceramic heating elements provide the heating. Heating elements are controlled by a custom computer program which regulates the temperature based on the reading of 20 K-type thermocouples mounted around the CARME chamber. The code slowly ramps the temperature by a maximum of 7 °C per hour while limiting thermal gradients across the chamber to minimise thermal stresses and ensure even baking across the chamber.

4.3. Achieving XHV with an empty vessel

Initial vacuum tests were conducted with no instrumentation or internal components installed, except for the vacuum pumps. The aim was to assess the minimum pressure achievable and confirm the good condition of the vacuum vessels. A single MAGW 300i turbo-molecular pump was mounted on top of the chamber, behind one of the two all-metal gate valves, and connected to an Edwards nXDS10 scroll pump. Following five days, the CARME vessel pressure reached 5×10^{-8} mbar. The CARME chamber was then baked (see Fig. 9) for two weeks at a maximum temperature of 140 °C after which, and while still at 140 °C, the chamber pressure had decreased to 6×10^{-9} mbar. UHV1400 NEG elements, connected in series in groups of two or three modules, were activated 4–5 modules at a time. NEG elements were not all activated at the same time in order to reduce the out-gassing load on the single turbo. D2000 NEG elements were activated at a temperature of 550 °C

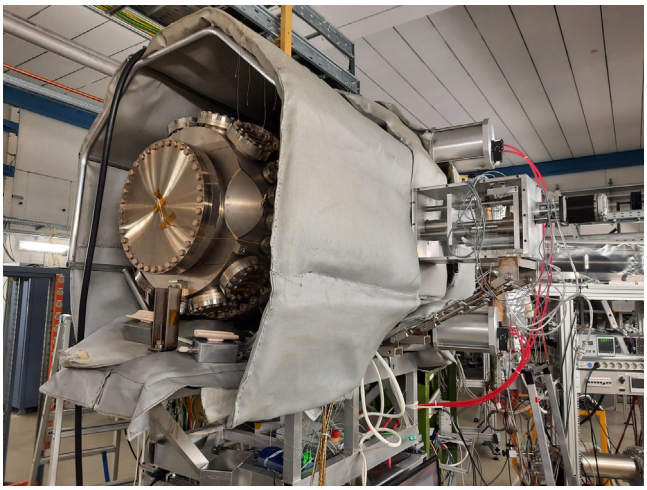

Fig. 8. Photo of the baking tent being installed around CARME. Note the multiple layers and the ceramic heating elements located at bottom of the chamber.

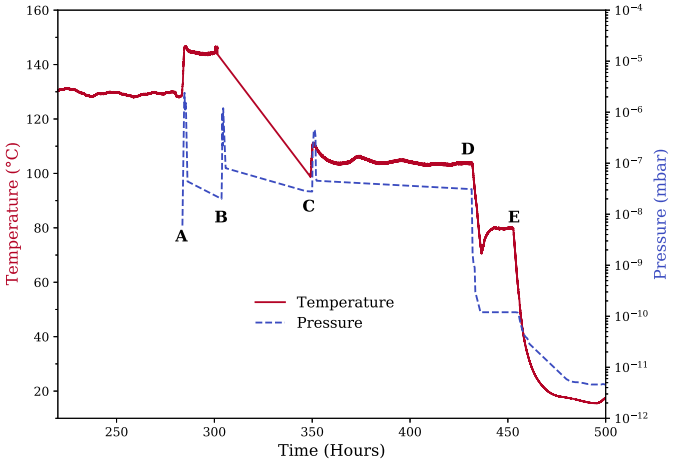

Fig. 9. Bake-out temperature and chamber pressure plot against time during XHV commissioning with an empty vessel in STFC Daresbury Laboratory. The temperature is taken as the average of all the chamber thermocouples and the chamber pressure is read from the hot cathode gauge mounted on the chamber. The hot-cathode gauge was not active during bake-out before NEG activation. The chamber was baked for ~280 h before NEG activation. Activation of NEG elements (A,B,C) produce a significant increase in pressure within the chamber. The surface of the NEG pumps were kept clean and conditioned by maintaining in low power mode post activation until time (D). The bake-out temperature is reduced in two stages (D,E). At room temperature, a pressure of 5×10^{-12} mbar was achieved.

which corresponds to a power of 170 W. The UHV1400 NEG elements did not have an internal temperature sensor and were activated with a power of 200 W per module. Post activation, the NEG elements were held at 200 °C for one week to increase diffusion into the bulk of the getter and ensure that NEG pump surfaces were not inhibited by the out-gassing of surrounding NEG elements during their activation cycle. The pressure increased to 1×10^{-6} mbar during the activation procedure, falling to 8×10^{-8} mbar while being maintained at 200 °C. The chamber temperature was maintained at 140 °C throughout the activation procedure via the tent heaters. The temperature was slowly reduced following activation. When the temperature reached values below 80 °C, ion pumps were turned on for 30 s at a time, four times. XHV pressures were achieved within hours of the chamber cooling to room temperature. The ultimate pressure achieved was around 5×10^{-12} mbar according to the IE514 hot cathode gauge. This pressure was maintained for several days before the system was re-pressurised with dry nitrogen for shipment to GSI/FAIR. An upper limit on the out-gassing rate of $\sim 3 \times 10^{-12}$ mbar(l/s)cm^{-2} for the empty vessel can be estimated by comparing the ultimate pressure achieved, the pumping speed installed in the chamber (26,200 l/s) and the internal surface area of the chamber.

4.4. Achieving XHV with a vacuum load

CARME was installed in the experimental section (YR09) on the CRYRING in September 2021. The chamber was vacuum tested with a full vacuum load, except detectors, before installation of the interaction chamber and gas-jet target in the section. The vacuum load consisted primarily of the 261 m of Kapton-insulated wire meant to eventually connect the DSSDs to the signal feed-throughs. The end of the Kapton wires connected to the MACOR leads that would plug in the DSSDs were left resting on the bottom of the vacuum chamber with the other end connected to signal feed-throughs. Three XHV-compatible Allectra thermocouples were placed inside the chamber, one attached to the Kapton wire bundles resting on the bottom of CARME and two left floating to monitor internal temperatures. The vacuum testing procedure was similar to that used at STFC Daresbury laboratory. Mechanical conflicts with the ring instrumentation around CARME reduced the efficiency of the insulating jacket and restricted the maximum baking temperature for the first three days to 90 °C. Additional insulating sections were installed during a brief pause in baking such that baking could continue at a temperature of 130 °C (see Fig. 10). Baking was conducted at 130 °C for ~ 6 days. During this period a power cut temporarily halted baking for several hours. The pressure following this bake-out period was 1.3×10^{-7} mbar. The temperature was reduced to 95 °C and the ion pumps were flashed on/off to de-gas. Activation of the NEG elements was then conducted in the same way as in Daresbury (two groups of 4–5 modules at a time). The activation procedure caused an increase in the internal temperature of the Kapton-insulated wires bundles to around 180 °C. Activation was halted, since a temperature above ≈150 °C would have destroyed the detectors had any been installed at this point.

Detailed tests of how to activate the NEG elements without producing excessive temperatures were conducted. The aim of these NEG activation tests was to establish a suitable procedure for activation of NEG modules while maintaining internal temperatures well below 150 °C. Testing consisted of activating either single NEG modules or small groups of NEG modules at different temperatures to gauge the effect on internal temperatures. No significant rise (>5–10 °C) of the temperature of internal thermocouples was observed until the temperature of the NEG element is above approximately 400 °C. The distance of NEG modules from the internal thermocouples also influenced the temperature rise observed. Large temperature increases were observed for elements activated last, even if the distance to the thermocouples was large. The likely cause is the cumulative power output of NEG elements that had been activated and were left at low power to condition them and keep them clean. A procedure for activation of NEG elements was determined during testing. First, each of the SAES D2000 NEG/Ion pumps were activated at around 400 °C for 90 min. Then, the UHV1400 NEG elements were activated one group (of 2 or 3 elements connected in series) at a time for 90 min. NEG elements close to detectors were activated last. UHV1400s far from the detectors were activated with a power of 100–150 W per module. UHV1400s close to detectors were activated with powers of 30–60 W of power per module. Power was slowly increased by 5–10 W to gauge the effect on internal temperatures. Following this procedure, all NEG modules were activated without the internal temperature exceeding 130 °C. The bake-out temperature can also be reduced prior to NEG activation to help prevent temperatures exceeding 130 °C. Following activation testing, ion pumps were turned on and the temperature reduced by ~ 10 °C per hour. An XHV pressure level of 9×10^{-12} mbar was achieved after the chamber cooled down at room temperature.

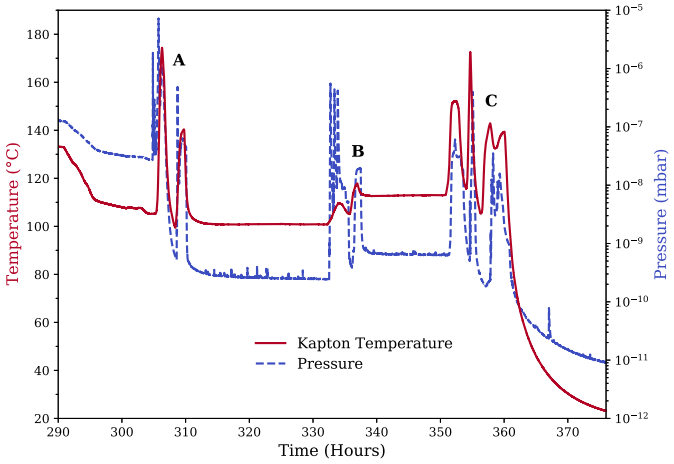

Fig. 10. Temperature of internal Kapton bundle and the chamber pressure plot against time for NEG activation testing period with no detectors inside the chamber. NEG activation testing was conducted over several days in three batches (A,B,C). NEG modules were initially activated 4–5 modules at a time and ∼ 170 W per module (A). Internal temperatures were too high with this methodology. Testing of different activation procedures was trialled (B,C). Following activation, NEG pump surfaces were kept clean and conditioned by maintaining in low power mode. Temperatures for the final NEG activations (C) are higher due to cumulative heating power of all NEG modules in low power mode.

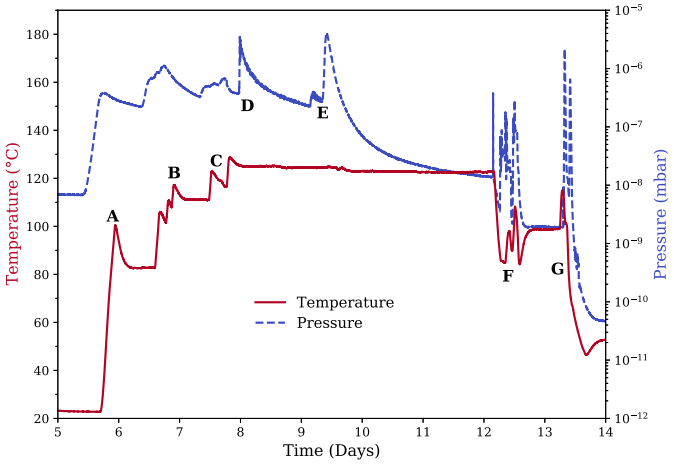

Fig. 11. Bake-out temperature and chamber pressure plot against time for the final bake-out with detectors installed. The temperature is taken as the average of chamber thermocouples. The time is shown from the fifth day of bake-out where consistent heating of the chamber was achieved. The temperature was increased in stages (A,B,C) up to 125 °C. The chamber pressure mirrors the increase in bake-out temperature. NEG modules were conditioned at low power resulting in two large pressure spikes (D,E). Little effect is observed in the temperature from the conditioning. Full activation of NEG modules (F,G) at a lower bake-out temperature, results in large pressure increases.

4.5. Achieving operational XHV at CRYRING

The procedure to achieve operational XHV, after final installation of detectors and the gas-jet target, was slightly different to the previous vacuum testing. The procedure was modified due to new mechanical constraints, introduced by full installation of the gas-jet target, as well as time constraints to allow for beam testing, and a different heating system due to a failure of the heating elements shown in Fig. 8. Due to the heater failure, the CARME chamber was wrapped in heating wires. A 10 m Heating wire was wrapped around the body of the CARME chamber providing 2000 W of power. The insulating jacket was reassembled around the CARME chamber with a small insulating jacket fitted to the bellows either side of the CARME chamber. Two 100 W CF100 "heating flanges" were installed on the bottom flanges of the intermediate section in addition to one 100 W CF100 on the bottom of the moving detector section. An additional 40 W CF100 was also installed on a lower flange of the intermediate section. Each heating element could be independently and manually controlled with a set-point temperature. Baking was no longer controlled by the automatic baking code. The heating wires increased the temperature by 0.2 °C per minute with temperature set-points chosen to maintain even baking across the chamber. Baking was started initially with only the 2000 W heating wire at a pressure of $\approx 1 \times 10^{-7}$ mbar (see Fig. 11). This setup provided insufficient and uneven heating such that the additional heating elements were added. The maximum average chamber temperature during this period was 90 °C for 12 h. Baking was restarted following the installation of additional heating elements at a pressure of $\approx 7.5\times 10^{-9}$ mbar. Bake-out was conducted with temperature set-points between 150 °C and 160 °C, but actually only reached a temperature of ∼ 120 °C. 72 h after baking was restarted, the D2000 NEG elements were conditioned with temperatures of 150 °C. A large increase in pressure was visible due to the conditioning procedure, but a minimal effect on the temperature was observed. The next day the UHV1400 NEG elements were activated at 20 W with minimal effect on temperature but a significant spike in pressure. Baking continued with NEG elements on low power for ∼ 7 days during which the pressure had dropped to $\approx 1 \times 10^{-8}$ mbar at 125 °C. Heating of all NEG modules was stopped and temperature set-points were reduced to 120 °C causing a drop in the average chamber temperature to 90 °C. Ion pumps were turned on for 30 s, five times each. D2000 NEG elements were activated first at 400 °C. The power was increased over 30 min and held for 90 min at temperature. After activation D2000s were held at a temperature of 200 °C. UHV1400s were activated in batches of two elements at a time between 200–250 W (100–125 W per module) with the NEG elements furthest from the detectors activated first. If temperatures began to climb significantly the power was reduced. UHV1400 modules closest to the detectors were activated consecutively with powers of 30–40 W per module. Ion pumps were turned on below 100 °C and heating power reduced following activation. The final pressure reached was ∼ 3×10^{-11} mbar. The total baking time was around 14 days, however due to issues with heating only ∼6 days with the chamber >100 °C was utilised with an additional 2 days for the NEG activation procedure. It is expected vacuum pressures $< 1 \times 10^{-11}$ mbar will be achieved in the future, even with detectors under vacuum, when using the baking equipment and procedure used in the previous Section 4.4.

5. Future prospects

CARME and its detectors were commissioned with stable beam in February-March 2022 as part of the GSI E141 experiment. Results are being analysed and will be the topic of a future publication. CARME is the first array of its kind and its design and commissioning will inform future similar devices that could be installed at other low-energy rings world-wide, including *e.g.* TRIUMF [11] and CERN [12]. Going forward, the science programme at CARME will be supported by the ELDAR (burning questions on the origin of the Elements in the Lives and Deaths of stARs) ERC Starting Grant (PI C.G. Bruno). ELDAR will pioneer new techniques and new approaches for this novel way of investigating reactions using heavy ions at storage rings. First experiments are expected to make use of stable beams to develop and refine the methodology, with radioactive beam campaigns to follow. In the near future CARME's programme will focus in particular on an exciting programme of direct reaction measurements, such as *e.g.* (p, α) or (α,p), using CARME downstream of the interaction chamber to investigate astrophysical sites ranging from quiescent burning stars, to novae and supernovae. The imminent installation at CRYRING of the FISIC transverse beam line [41] will give the opportunity to study nuclear reactions by crossing the beam stored in the ring with CARME and the FISIC transverse beam. This will allow first ever measurement

of nuclear reactions free of electron screening directly at energies of astrophysical interest as part of ELDAR (GSI proposal G22-87). Electron screening is a long-standing puzzle [42] that affects knowledge all nuclear reactions taking place in quiescent scenarios, including in particular our own Sun. In the longer term CARME is planned to be moved upstream of the interaction chamber and employed for transfer reaction studies using approaches such as (d,p), and also in the future potentially coincidence measurements with a 0 degree system similar to that already operational at the ESR [10]. Many of these experiments will be the first of their kind, opening up the path for exploitation of low-energy heavy-ion storage rings, and targeting long-standing puzzles for a rich programme of low-energy nuclear physics and nuclear astrophysics experiments.

Declaration of competing interest

The authors declare that they have no known competing financial interests or personal relationships that could have appeared to influence the work reported in this paper.

Data availability

Data will be made available on request.

Acknowledgements

CARME was designed, built and commissioned thanks to the funding provided by UK STFC via the ISOL-SRS grant (Project ST/M001652/1). J.G., Yu. L. and T. S. also gratefully acknowledge support by the State of Hesse within the Research Cluster ELEMENTS (Project ID 500/10.006).

References

[1] M. Steck, Y.A. Litvinov, Heavy-ion storage rings and their use in precision experiments with highly charged ions, Prog. Part. Nucl. Phys. 115 (2020) 103811, http://dx.doi.org/10.1016/j.ppnp.2020.103811, URL https://www.sciencedirect.com/science/article/pii/S0146641020300582.

[2] H. Moeini, S. Ilieva, F. Aksouh, K. Boretzky, A. Chatillon, A. Corsi, P. Egelhof, H. Emling, G. Ickert, J. Jourdan, N. Kalantar Nayestanaki, D. Kiselev, O. Kiselev, C. Kozhuharov, T. Le Bleis, X. Le, Y. Litvinov, K. Mahata, J. Meier, F. Nolden, S. Paschalis, U. Popp, H. Simon, M. Steck, T. Stöhlker, H. Weick, D. Werthmüller, A. Zalite, First feasibility experiment for the EXL project with prototype detectors at the ESR storage ring, Nucl. Instrum. Methods Phys. Res. A 634 (1) (2011) 77–84, http://dx.doi.org/10.1016/j.nima.2011.01.036, URL https://www.sciencedirect.com/science/article/pii/S0168900211000878.

[3] M. Mutterer, P. Egelhof, V. Eremin, S. Ilieva, N. Kalantar Nayestanaki, O. Kiselev, H. Kollmus, T. Kröll, M. Kuilman, L.X. Chung, Experimental techniques for in-ring reaction experiments, Phys. Scr. 2015 (T166) (2015) http://dx.doi.org/10.1088/0031-8949/2015/T166/014053, URL https://iopscience.iop.org/article/10.1088/0031-8949/2015/T166/014053.

[4] J. Zamora, T. Aumann, S. Bagchi, S. Bönig, M. Csatlós, I. Dillmann, C. Dimopoulou, P. Egelhof, V. Eremin, T. Furuno, H. Geissel, R. Gernhäuser, M. Harakeh, A.-L. Hartig, S. Ilieva, N. Kalantar-Nayestanaki, O. Kiselev, H. Kollmus, C. Kozhuharov, A. Krasznahorkay, T. Kröll, M. Kuilman, S. Litvinov, Y. Litvinov, M. Mahjour-Shafiei, M. Mutterer, D. Nagae, M. Najafi, C. Nociforo, F. Nolden, U. Popp, C. Rigollet, S. Roy, C. Scheidenberger, M. von Schmid, M. Steck, B. Streicher, L. Stuhl, M. Thürauf, T. Uesaka, H. Weick, J. Winfield, D. Winters, P. Woods, T. Yamaguchi, K. Yue, J. Zenihiro, First measurement of isoscalar giant resonances in a stored-beam experiment, Phys. Lett. B 763 (2016) 16–19, http://dx.doi.org/10.1016/j.physletb.2016.10.015, URL https://www.sciencedirect.com/science/article/pii/S037026931630586X.

[5] J.C. Zamora, T. Aumann, S. Bagchi, S. Bönig, M. Csatlós, I. Dillmann, C. Dimopoulou, P. Egelhof, V. Eremin, T. Furuno, H. Geissel, R. Gernhäuser, M.N. Harakeh, A.-L. Hartig, S. Ilieva, N. Kalantar-Nayestanaki, O. Kiselev, H. Kollmus, C. Kozhuharov, A. Krasznahorkay, T. Kröll, M. Kuilman, S. Litvinov, Y.A. Litvinov, M. Mahjour-Shafiei, M. Mutterer, D. Nagae, M.A. Najafi, C. Nociforo, F. Nolden, U. Popp, C. Rigollet, S. Roy, C. Scheidenberger, M. von Schmid, M. Steck, B. Streicher, L. Stuhl, M. Thürauf, T. Uesaka, H. Weick, J.S. Winfield, D. Winters, P.J. Woods, T. Yamaguchi, K. Yue, J. Zenihiro, Nuclear-matter radius studies from ^{58}Ni(α,α) experiments at the GSI experimental storage ring with the EXL facility, Phys. Rev. C 96 (2017) 034617, http://dx.doi.org/10.1103/PhysRevC.96.034617, URL https://link.aps.org/doi/10.1103/PhysRevC.96.034617.

[6] M. von Schmid, S. Bagchi, S. Bönig, M. Csatlós, I. Dillmann, C. Dimopoulou, P. Egelhof, V. Eremin, T. Furuno, H. Geissel, R. Gernhäuser, M.N. Harakeh, A.-L. Hartig, S. Ilieva, N. Kalantar-Nayestanaki, O. Kiselev, H. Kollmus, C. Kozhuharov, A. Krasznahorkay, T. Kröll, M. Kuilman, S. Litvinov, Y.A. Litvinov, M. Mahjour-Shafiei, M. Mutterer, D. Nagae, M.A. Najafi, C. Nociforo, F. Nolden, U. Popp, C. Rigollet, S. Roy, C. Scheidenberger, M. Steck, B. Streicher, L. Stuhl, M. Thürauf, T. Uesaka, H. Weick, J.S. Winfield, D. Winters, P.J. Woods, T. Yamaguchi, K. Yue, J.C. Zamora, J. Zenihiro, for the EXL collaboration, Investigation of the nuclear matter distribution of ^{56}Ni by elastic proton scattering in inverse kinematics, Phys. Scr. T166 (2015) 014005, http://dx.doi.org/10.1088/0031-8949/2015/t166/014005.

[7] K. Yue, J.T. Zhang, X.L. Tu, C.J. Shao, H.X. Li, P. Ma, B. Mei, X.C. Chen, Y.Y. Yang, X.Q. Liu, Y.M. Xing, K.H. Fang, X.H. Li, Z.Y. Sun, M. Wang, P. Egelhof, Y.A. Litvinov, K. Blaum, Y.H. Zhang, X.H. Zhou, Measurement of ^{58}Ni$(p,p)^{58}$Ni elastic scattering at low momentum transfer by using the HIRFL-CSR heavy-ion storage ring, Phys. Rev. C 100 (2019) 054609, http://dx.doi.org/10.1103/PhysRevC.100.054609, URL https://link.aps.org/doi/10.1103/PhysRevC.100.054609.

[8] D. Doherty, P. Woods, Y.A. Litvinov, M.A. Najafi, S. Bagchi, S. Bishop, M. Bo, C. Brandau, T. Davinson, I. Dillmann, et al., Nuclear transfer reaction measurements at the ESR—for the investigation of the astrophysical 15o (α,γ) 19Ne reaction, Phys. Scr. 2015 (T166) (2015) 014007.

[9] B. Mei, T. Aumann, S. Bishop, K. Blaum, K. Boretzky, F. Bosch, C. Brandau, H. Bräuning, T. Davinson, I. Dillmann, C. Dimopoulou, O. Ershova, Z. Fülöp, H. Geissel, J. Glorius, G. Gyürky, M. Heil, F. Käppeler, A. Kelic-Heil, C. Kozhuharov, C. Langer, T. Le Bleis, Y. Litvinov, G. Lotay, J. Marganiec, G. Münzenberg, F. Nolden, N. Petridis, R. Plag, U. Popp, G. Rastrepina, R. Reifarth, B. Riese, C. Rigollet, C. Scheidenberger, H. Simon, K. Sonnabend, M. Steck, T. Stöhlker, T. Szücs, K. Sümmerer, G. Weber, H. Weick, D. Winters, N. Winters, P. Woods, Q. Zhong, First measurement of the ^{96}Ru$(p,\gamma)^{97}$Rh cross section for the p process with a storage ring, Phys. Rev. C 92 (2015) 035803, http://dx.doi.org/10.1103/PhysRevC.92.035803, URL https://link.aps.org/doi/10.1103/PhysRevC.92.035803.

[10] J. Glorius, C. Langer, Z. Slavkovská, L. Bott, C. Brandau, B. Brückner, K. Blaum, X. Chen, S. Dababneh, T. Davinson, P. Erbacher, S. Fiebiger, T. Gaß ner, K. Göbel, M. Groothuis, A. Gumberidze, G. Gyürky, M. Heil, R. Hess, R. Hensch, P. Hillmann, P.-M. Hillenbrand, O. Hinrichs, B. Jurado, T. Kausch, A. Khodaparast, T. Kisselbach, N. Klapper, C. Kozhuharov, D. Kurtulgil, G. Lane, C. Lederer-Woods, M. Lestinsky, S. Litvinov, Y.A. Litvinov, B. Löher, F. Nolden, N. Petridis, U. Popp, T. Rauscher, M. Reed, R. Reifarth, M.S. Sanjari, D. Savran, H. Simon, U. Spillmann, M. Steck, T. Stöhlker, J. Stumm, A. Surzhykov, T. Szücs, T.T. Nguyen, A. Taremi Zadeh, B. Thomas, S.Y. Torilov, H. Törnqvist, M. Träger, C. Trageser, S. Trotsenko, L. Varga, M. Volknandt, H. Weick, M. Weigand, C. Wolf, P.J. Woods, Y.M. Xing, Approaching the gamow window with stored ions: Direct measurement of ^{124}Xe(p,γ) in the ESR storage ring, Phys. Rev. Lett. 122 (2019) 092701, http://dx.doi.org/10.1103/PhysRevLett.122.092701, URL https://link.aps.org/doi/10.1103/PhysRevLett.122.092701.

[11] P. Navrátil, ARIEL experiments and theory, J. Phys.: Conf. Ser. 2391 (2022) 012002, http://dx.doi.org/10.1088/1742-6596/2391/1/012002.

[12] M. Grieser, Y.A. Litvinov, R. Raabe, K. Blaum, Y. Blumenfeld, P.A. Butler, F. Wenander, P.J. Woods, M. Aliotta, A. Andreyev, A. Artemyev, D. Atanasov, T. Aumann, D. Balabanski, A. Barzakh, L. Batist, A.P. Bernardes, D. Bernhardt, J. Billowes, S. Bishop, M. Borge, I. Borzov, F. Bosch, A.J. Boston, C. Brandau, W. Catford, R. Catherall, J. Cederkäll, D. Cullen, T. Davinson, I. Dillmann, C. Dimopoulou, G. Dracoulis, C.E. Düllmann, P. Egelhof, A. Estrade, D. Fischer, K. Flanagan, L. Fraile, M.A. Fraser, S.J. Freeman, H. Geissel, J. Gerl, P. Greenlees, R.E. Grisenti, D. Habs, R. von Hahn, S. Hagmann, M. Hausmann, J.J. He, M. Heil, M. Huyse, D. Jenkins, A. Jokinen, B. Jonson, D.T. Joss, Y. Kadi, N. Kalantar-Nayestanaki, B.P. Kay, O. Kiselev, H.J. Kluge, M. Kowalska, C. Kozhuharov, S. Kreim, T. Kröll, J. Kurcewicz, M. Labiche, R.C. Lemmon, M. Lestinsky, G. Lotay, X.W. Ma, M. Marta, J. Meng, D. Mücher, I. Mukha, A. Müller, A.S.J. Murphy, G. Neyens, T. Nilsson, C. Nociforo, W. Nörtershäuser, R.D. Page, M. Pasini, N. Petridis, N. Pietralla, M. Pfützner, Z. Podolyák, P. Regan, M.W. Reed, R. Reifarth, P. Reiter, R. Repnow, K. Riisager, B. Rubio, M.S. Sanjari, D.W. Savin, C. Scheidenberger, S. Schippers, D. Schneider, R. Schuch, D. Schwalm, L. Schweikhard, D. Shubina, E. Siesling, H. Simon, J. Simpson, J. Smith, K. Sonnabend, M. Steck, T. Stora, T. Stöhlker, B. Sun, A. Surzhykov, F. Suzaki, O. Tarasov, S. Trotsenko, X.L. Tu, P. Van Duppen, C. Volpe, D. Voulot, P.M. Walker, E. Wildner, N. Winckler, D.F.A. Winters, A. Wolf, H.S. Xu, A. Yakushev, T. Yamaguchi, Y.J. Yuan, Y.H. Zhang, K. Zuber, Storage ring at HIE-ISOLDE. Technical design report, Eur. Phys. J. Spec. Top. 207 (2012) 1–117, http://dx.doi.org/10.1140/epjst/e2012-01599-9.

[13] M. Lestinsky, V. Andrianov, B. Aurand, V. Bagnoud, D. Bernhardt, H. Beyer, S. Bishop, K. Blaum, A. Bleile, A. Borovik, F. Bosch, C.J. Bostock, C. Brandau, A. Bräuning-Demian, I. Bray, T. Davinson, B. Ebinger, A. Echler, P. Egelhof, A. Ehresmann, M. Engström, C. Enss, N. Ferreira, D. Fischer, A. Fleischmann, E. Förster, S. Fritzsche, R. Geithner, S. Geyer, J. Glorius, K. Göbel, O. Gorda, J. Goullon, P. Grabitz, R. Grisenti, A. Gumberidze, S. Hagmann, M. Heil, A. Heinz, F. Herfurth, R. Heß, P.M. Hillenbrand, R. Hubele, P. Indelicato, A. Källberg, O. Kester, O. Kiselev, A. Knie, C. Kozhuharov, S. Kraft-Bermuth, T. Kühl, G. Lane, Y.A. Litvinov, D. Liesen, X.W. Ma, R. Märtin, R. Moshammer, A. Müller,

S. Namba, P. Neumeyer, T. Nilsson, W. Nörtershäuser, G. Paulus, N. Petridis, M. Reed, R. Reifarth, P. Reiß, J. Rothhardt, R. Sanchez, M.S. Sanjari, S. Schippers, H.T. Schmidt, D. Schneider, P. Scholz, R. Schuch, M. Schulz, V. Shabaev, A. Simonsson, J. Sjöholm, Ö. Skeppstedt, K. Sonnabend, U. Spillmann, K. Stiebing, M. Steck, T. Stöhlker, A. Surzhykov, S. Torilov, E. Träbert, M. Trassinelli, S. Trotsenko, X.L. Tu, I. Uschmann, P.M. Walker, G. Weber, D.F.A. Winters, P.J. Woods, H.Y. Zhao, Y.H. Zhang, Physics book: CRYRING@ESR, Eur. Phys. J. Spec. Top. 225 (5) (2016) http://dx.doi.org/10.1140/epjst/e2016-02643-6.

[14] M. Lestinsky, E.B. Menz, H. Danared, C. Krantz, E. Lindroth, Z. Andelkovic, C. Brandau, A. Bräuning-Demian, S. Fedotova, W. Geithner, F. Herfurth, A. Kalinin, I. Kraus, U. Spillmann, G. Vorobjev, T. Stöhlker, SPARC, the CRYRING@ESR collaboration, First experiments with CRYRING@ESR, in: 20th International Conference on the Physics of Highly Charged Ions, Atoms (2023) submitted for publication.

[15] M. Lestinsky, N. Angert, R. Bär, R. Becker, M. Bevcic, U. Blell, W. Bock, A. Bräuning-Demian, H. Danared, O. Dolinskyy, W. Enders, M. Engström, A. Fischer, B. Franzke, G. Gruber, P. Hülsmann, A. Källberg, O. Kester, C.-M. Kleffner, Y.A.L. amd Carsten Mühle, B. Müller, I. Pschorn, T. Radon, H. Ramakers, H. Reich-Sprenger, D. Reistad, G. Riefert, M. Schwickert, A. Simonsson, J. Sjöholm, Ö. Skeppstedt, M. Steck, T. Stöhlker, W. Vinzenz, H. Welker, CRYRING@ESR: A study group report, Project study, GSI, Darmstadt, 2012, URL https://www.gsi.de/fileadmin/SPARC/documents/Cryring/ReportCryring_40ESR.PDF.

[16] F. Herfurth, Z. Andelkovic, M. Bai, A. Bräuning-Demian, V. Chetvertkova, O. Geithner, W. Geithner, O. Gorda, A. Källberg, M. Lestinsky, S. Litvinov, T. Stöhlker, G. Vorobjev, U. Weinrich, Commissioning of the low energy storage ring facility CRYRING@ESR, in: Proc. of Workshop on Beam Cooling and Related Topics (COOL'17), Bonn, Germany, 18-22 September 2017, in: Workshop on Beam Cooling and Related Topics, (11) JACoW, Geneva, Switzerland, 2018, pp. 81–83, http://dx.doi.org/10.18429/JACoW-COOL2017-THM13, URL http://jacow.org/cool2017/papers/thm13.pdf.

[17] FAIR, 2022 URL https://fair-center.eu, (Accessed 11 2022).

[18] P. Spiller, M. Bai, J. Blaurock, O. Boine-Frankenheim, A. Dolinskii, F. Hagenbuck, C. Kleffner, K. Knie, I. Koop, S. Menke, et al., Status of the FAIR project, in: Proc. 9th, 2018.

[19] P.J. Woods, et al., ISOL-SRS: ISOL beam storage ring spectrometer, 2015, STFC Project ST/M001652/1.

[20] O. Forstner, D. Bemmerer, T.E. Cowan, R. Dressler, A.R. Junghans, D. Schumann, T. Stöhlker, T. Szücs, A. Wagner, K. Zuber, Opportunities for measurements of astrophysical-relevant alpha-capture reaction rates at CRYRING@ESR, X-Ray Spectrometry 49 (1) (2020) 129–132, http://dx.doi.org/10.1002/xrs.3071.

[21] A.S. Schlachter, J.W. Stearns, W.G. Graham, K.H. Berkner, R.V. Pyle, J.A. Tanis, Electron capture for fast highly charged ions in gas targets: An empirical scaling rule, Phys. Rev. A 27 (1983) 3372–3374, http://dx.doi.org/10.1103/PhysRevA.27.3372, URL https://link.aps.org/doi/10.1103/PhysRevA.27.3372.

[22] N. Petridis, R.E. Grisenti, Y.A. Litvinov, T. Stöhlker, Prototype internal target design for storage ring experiments, Phys. Scr. T166 (2015) 014051, http://dx.doi.org/10.1088/0031-8949/2015/t166/014051.

[23] C. Krantz, Z. Andelkovic, C. Brandau, C. Dimopoulou, W. Geithner, T. Hackler, V. Hannen, F. Herfurth, R. Hess, M. Lestinsky, E. Menz, A. Reiter, J. Roßbach, S. Schippers, C. Schroeder, A. Täschner, G. Vorobjev, C. Weinheimer, D. Winzen, Recommissioning of the CRYRING@ESR electron cooler, in: Proceedings of the 12th International Particle Accelerator Conference, vol. IPAC2021, JACoW Publishing, Geneva, Switzerland, 2021, pp. 1816–1818, http://dx.doi.org/10.18429/JACOW-IPAC2021-TUPAB178.

[24] ITL vacuum components, 2022, URL https://www.itl-vacuum.com/, (Accessed 10 2022).

[25] Micron semiconductors ltd, 2022, URL http://www.micronsemiconductor.co.uk, (Accessed 10 2022).

[26] Rogers, 2022. URL www.rogerscorp.com/advanced-electronics-solutions/ro4000-series-laminates/ro4003c-laminates, (Accessed 10 2022).

[27] Festo Ltd, 2022, URL https://www.festo.com, (Accessed 10 2022).

[28] Teknic Inc, 2022, URL https://teknic.com/. (Accessed 10 2022).

[29] O. Hall, T. Davinson, C.J. Griffin, C. Appleton, C.G. Bruno, A. Estrade, D. Kahl, L. Sexton, P.J. Woods, I. Burrows, P.J. Coleman-Smith, M. Cordwell, A. Grant, M. Kogimtzis, M. Labiche, J. Lawson, I. Lazarus, V.F.E. Pucknell, J. Simpson, C. Unsworth, D. Braga, M. Prydderch, S.L. Thomas, L.J. Harkness-Brennan, P.J. Nolan, D. Seddon, R.D. Page, The advanced implantation detector array (AIDA), Nucl. Inst. Phys. A (2022) submitted for publication.

[30] V.F.E. Pucknell, et al., 2022 URL http://npg.dl.ac.uk/MIDAS/. (Accessed 11 2022).

[31] Allectra gmbh, 2022, URL https://www.allectra.com/. (Accessed 10 2022).

[32] V.H. K. Battes, Outgassing behavior of different high-temperature resistant polymers, J. Vacuum Sci. Technol. A Vacuum Surf. Films 36 (2018) http://dx.doi.org/10.1116/1.5001243.

[33] R. Peacock, Practical selection of elastomer materials for vacuum seals, J. Vacuum Sci. Technol. 17 (1980) http://dx.doi.org/10.1116/1.570380.

[34] Leybold, 2022, URL https://www.leybold.com, (Accessed 10 2022).

[35] VAT Group AG, 2022, URL https://www.vatvalve.com, (Accessed 10 2022).

[36] Edwards, 2022, URL https://www.edwardsvacuum.com, (Accessed 10 2022).

[37] SAES getters spa, 2022, URL https://www.saesgetters.com/, (Accessed 10 2022).

[38] K. Jousten, C.B. Nakhosteen, Handbook of Vacuum Technology, 2nd, John Wiley and Sons Incorporated, 2016.

[39] R. Reid, Vacuum systems, procedures for cleaning of vacuum items, 2003, https://www2.ph.ed.ac.uk/~td/isol-srs/spc-003-CleaningofVacuumItems.pdf.

[40] J.F. O'Hanlon, A User's Guide to Vacuum Technology, 3rd, John Wiley and Sons Incorporated, 2003.

[41] D. Schury, A. Méry, J.M. Ramillon, L. Adoui, J.-Y. Chesnel, A. Lévy, S. Macé, C. Prigent, J. Rangama, P. Rousseau, S. Steydli, M. Trassinelli, D. Vernhet, A. Gumberidze, T. Stöhlker, A. Bräuning-Demian, C. Hahn, U. Spillmann, E. Lamour, The low energy beamline of the FISIC experiment: current status of construction and performance, J. Phys. Conf. Ser. 1412 (16) (2020) 162011, http://dx.doi.org/10.1088/1742-6596/1412/16/162011.

[42] M. Aliotta, K. Langanke, Screening effects in stars and in the laboratory, Front. Phys. 10 (2022) http://dx.doi.org/10.3389/fphy.2022.942726, URL https://www.frontiersin.org/articles/10.3389/fphy.2022.942726.